Journal of Innovative Optical Health Sciences
Vol. 4, No. 3 (2011) 325–335
© World Scientific Publishing Company
DOI: 10.1142/S1793545811001599

World Scientific
www.worldscientific.com

HIGH-SPEED SPECTRAL DOMAIN OPTICAL COHERENCE TOMOGRAPHY SIGNAL PROCESSING WITH TIME-DOMAIN INTERPOLATION USING GRAPHICS PROCESSING UNIT

XIQI LI[*,†,‡], GUOHUA SHI[*,†,‡,¶], LING WEI[*,†,‡], ZHIHUA DING[§]
and YUDONG ZHANG[*,†]
[*]*The Laboratory on Adaptive Optics*
Institute of Optics and Electronics
Chinese Academy of Sciences, Chengdu 610209, China
[†]*The Key Laboratory on Adaptive Optics*
Chinese Academy of Sciences, Chengdu 610209, China
[‡]*Graduate School of Chinese Academy of Sciences*
Beijing 100080, China
[§]*State Key Laboratory of Modern Optical Instrumentation*
Zhejiang University, Hangzhou 310027, China
[¶]*guohua_shi@yahoo.com.cn*

Accepted 18 April 2011

Sensitivity and data processing speed are important in spectral domain Optical Coherence Tomography (SD-OCT) system. To get a higher sensitivity, zero-padding interpolation together with linear interpolation is commonly used to re-sample the interference data in SD-OCT, which limits the data processing speed. Recently, a time-domain interpolation for SD-OCT was proposed. By eliminating the huge Fast Fourier Transform Algorithm (FFT) operations, the operation number of the time-domain interpolation is much less than that of the zero-padding interpolation. In this paper, a numerical simulation is performed to evaluate the computational complexity and the interpolation accuracy. More than six times acceleration is obtained. At the same time, the normalized mean square error (NMSE) results show that the time-domain interpolation method with cut-off length $L = 21$ and $L = 31$ can improve about 1.7 dB and 2.1 dB when the distance mismatch is 2.4 mm than that of zero-padding interpolation method with padding times $M = 4$, respectively. Furthermore, this method can be applied the parallel arithmetic processing because only the data in the cut-off window is processed. By using Graphics Processing Unit (GPU) with compute unified device architecture (CUDA) program model, a frame (400 A-lines × 2048 pixels × 12 bits) data can be processed in 6 ms and the processing capability can be achieved 164,000 line/s for 1024-OCT and 71,000 line/s for 2048-OCT when the cut-off length is 21. Thus, a high-sensitivity and ultra-high data processing SD-OCT is realized.

Keywords: SD-DCT; time-domain interpolation; GPU; CUDA; data processing.

1. Introduction

Optical coherence tomography (OCT) is a noninvasive, cross-sectional optical imaging technique that allows for high-resolution, cross-sectional tomography imaging of the internal microstructure in materials and biological systems of backscatter or backreflected samples.[1–6] The first OCT is called Time Domain OCT (TD-OCT), in which low coherence interferometer with the scanning optical delay lines (ODLs) was used. An ameliorative modality called Fourier-domain OCT (FD-OCT) became more popular than TD-OCT owing to its significant advantages in imaging speed and detection sensitivity.[4,5] FD-OCT can be implemented by a swept laser source (swept source OCT, SS-OCT) or spectrometer-based system (Spectral Domain OCT, SD-OCT).[5,7–9] In SD-OCT systems, the depth information of sample is encoded into time-of-flight of the backscattered light and decoded by means of time cross-correlation with the original light.[6] The interference light is detected by a linescan camera. And then, the structure information of samples can be obtained by the data-processing the acquired interference signal. Comparing to other OCT techniques, SD-OCT is more simple and cost-saving, making SD-OCT an actively researched topic.[4]

Generally, both imaging speed and the imaging quality are required in many OCT applications. For example, some biological applications require real-time or even higher speed imaging. The high imaging speed can significantly reduce the motion artifacts and increase sampling density.[10,11] With the development of the linescan camera, the spectra acquisition speed can reach 312,500 lines/s, much faster than the data-processing speed that can be reached by the personal computer.[12]

Several resolutions have been applied to realize real-time data processing for OCT. Real-time optical coherence tomography processing is realized by using digital signal processing (DSP) or field-programmable gate-based array (FPGA).[13–15] But it would increase the system complexity and cost because additional hardware inclusions are needed. A real-time swept source polarization-sensitive OCT system by using OpenMP model has been reported,[16] but it is not suitable for a nonlinear-k space spectrometer needed in SD-OCT.

Recent advances in GPU provide a new way for parallel computation.[17,18] The computation capability of the GPU is now 10 times than that of the Central processing units (CPU).[17,18] With the compute-unified device architecture (CUDA) program model, the powerful GPU can be handled easily. The processing time of the SD-OCT system can be accelerated by the help of this tool.[19–21] A real-time four-dimensional (4D) signal processing and visualization using GPUs on a regular nonlinear-k Fourier-domain OCT system is reported.[20] They proposed a GPU accelerated linear spline interpolation (LSI) for λ-to-k resampling. The interpolation speed is more than 3,000,000 line/s for 1024-pixel OCT and more than 1,400,000 line/s for 2048-pixel OCT. But the LSI is not a good approach to improve the signal-to-noise ratio (SNR) of the OCT system. It is because that the k and λ have an inverse relationship of $k = 2\pi/\lambda$ and $\delta k = 2\pi\delta\lambda/\lambda^2$. So, the spectra in spectrometer must be nonlinearly resampled.[22] But the frequency oscillation period in spectrometer can be as small as two pixels, and any local interpolation scheme such as cubic spline is bound to fail.[23] Thus, zero-padding interpolation together with linear interpolation is commonly used in SD-OCT data resampling process.[12;23–25] However, this method greatly reduces the signal processing speed of the OCT system because of the huge FFT and logic operations, which has became a bottleneck of the high-sensitivity OCT system. A real-time processing system with zero-padding interpolation using multiple GPU was proposed.[21] The computing times for 2048 axial pixels × 1024 lateral A-lines were 26.88 ms and 14.75 ms by using a single GPU and dual GPUs, respectively. But all the data in one A-line are needed to get a point of resampled data in zero-padding interpolation. So it is not suitable for parallel algorithm. Furthermore, the interpolation interval in zero-padding is fixed. So, a linear interpolation must be appended to get the interference of an accurate wave number, which significantly reduces the interpolation accuracy.

A time-domain interpolation based on zero-padding has been reported recently.[2] This method can reduce a lot of processing time while it also gets better SNR comparing to the commonly used zero-padding method. The time-domain interpolation is performed by convoluting the interference data sequence and the cut-off coefficient in the time domain.[2] Thus, the interpolation processing only needs the interference data and the coefficient in the cut-off window, which have a loose relation with the whole data. So the whole processing of this method can be run in parallel. Therefore, GPU can be applied to accelerate the data processing. A high processing speed and high interpolation accuracy can be obtained by time-domain interpolation method. An ultra-high sensitivity and high data processing SD-OCT is realized.

This paper is structured as follows: In Sec. 2 the detail deduction of the proposed interpolation is presented. A cut-off window is added to accelerate the interpolation speed and its effect is discussed. In order to validate the discussion in Sec. 2, the numerical simulations are performed in Sec. 3 to evaluate the interpolation speed and accuracy by using the normalized mean square error (NMSE). The NMSE of the time-domain interpolation and the zero-padding interpolation is obtained for comparison. In Sec. 4 a SD-OCT setup and its data processing with CUDA model is described. The computing time of the data processing and the capability of the GPU are discussed. The conclusions of this work are drawn in Sec. 5.

2. Principle

In a SD-OCT system, the interference signal is detected by a linescan camera. Assume that the pixel number of the linescan camera is N in even and the signal detected by the linescan camera can be described as $x(n),\ n \in [0, N-1]$. Its frequency sequence $X[k]$ can be obtained by taking Discrete Fourier Transform algorithm (DFT) to $x(n)$. The zero-padding interpolation can be operated by following steps:

(1) Perform DFT of real sequence $x(n)$ to get a frequency domain's sequence $X[k]$;
(2) Increase the frequency domain's length to M times by zero-filling.

$$X_1(i') = \begin{cases} X(i'), & 0 \le i' \le \dfrac{N}{2} - 1 \\ 0, & \text{others} \\ X(i' - MN + N), & MN - \dfrac{N}{2} \le i' \le MN - 1 \end{cases} \tag{1}$$

(3) Perform DFT of $X_1(i')$ to time domain and get $x_1(n)$, where n ranges from 0 to $M \times N - 1$.
(4) A linear interpolation is added on to reshape $x_1(n)$ from $M \times N$ length to N length.

The signal acquired by the spectrometer of the SD-OCT is real-valued. The Fourier sequence $X[k]$ has the following characteristics because it is conjugate-symmetric.

$$X[m] = X^*[\langle -m \rangle_N], \tag{2}$$

$$\begin{aligned} \operatorname{Im} X(m) &= -\operatorname{Im} X^*(N-m), \\ \operatorname{Re} X(m) &= \operatorname{Re} X^*(N-m), \end{aligned} \tag{3}$$

where Im and *Re* are the imagery and real parts of $X(m)$. The symbol * denotes conjugate and $\langle m \rangle_N$ denotes periodic conjugate.

In SD-OCT applications, an N-length sequence is needed to perform FFT algorithm, so a linear interpolation is used to get reshape $x_1(n)$ from $M \times N$ length to N length. By doing so the accuracy of the resample processing is compromised.

In the proposed time-domain interpolation, a point was added to get a conjugate-symmetric form in Eq. (1).

$$X_2(i') = \begin{cases} X(i'), & 0 \le i' \le \dfrac{N}{2} \\ 0, & \text{others} \\ X(i' - MN + N), & MN - \dfrac{N}{2} \le i' \le MN - 1 \end{cases} \tag{4}$$

Transform the sequence $X_2(i')$ to time-domain by using inverse DFT. That is:

$$x_2(s) = \frac{1}{MN+1} \sum_{i'=0}^{MN-1} X_2(i') W_{MN}^{-i's}, \tag{5}$$

where $W_{MN} = \exp(-j\frac{2\pi}{MN})$, $x_2(s)$ is the new time domain sequence and s range from 0 to $M \times N - 1$. Because a point is added into the sequence, $M \times N + 1$ is needed to normalize the dataset. Referring to Eq. (4), $x_2(s)$ can be expressed as:

$$x_2(s) = \frac{1}{MN+1} \sum_{i'=0}^{N/2} X_2(i') W_{MN}^{-i's} + \frac{1}{MN+1} \times \sum_{i'=(MN-N/2)}^{MN-1} X_2(i') W_{MN}^{-i's}. \tag{6}$$

Let $l = i' - M \times N$ and substitute it into the second term, Eq. (6) can be expressed as:

$$x_2(s) = \frac{1}{MN+1} \left(X_2(0) + \sum_{i'=1}^{N/2} X_2(i') W_{MN}^{-i's} + \sum_{l=-(N/2)}^{-1} X_2(l + MN) W_{MN}^{-(l+MN)s} \right). \tag{7}$$

Noting that $X[l] = X^*[\langle -l\rangle_N]$, the last term in Eq. (7) can be deduced to:

$$x_2(s) = \frac{1}{MN+1}\left(X(0)+\sum_{j=1}^{N/2}X(j)W_{MN}^{-js} + \sum_{j=1}^{N/2}X(N-j)W_{MN}^{js}\right). \tag{8}$$

Referring to Eq. (3), Eq. (8) can be deduced to:

$$x_2(s) = \frac{1}{MN+1}\left(X(0)+\sum_{j=1}^{N/2}X(j)W_{MN}^{-js} + \sum_{j=1}^{N/2}X^*(-j)W_{MN}^{js}\right), \tag{9}$$

and then:

$$x_2(s) = \frac{1}{MN+1}X(0) + \frac{2}{MN+1}Re\left\{\sum_{j=1}^{N/2}X(j)W_{MN}^{-js}\right\}. \tag{10}$$

Referring to the definition of the DFT, Eq. (10) can be expressed as:

$$x_2(s) = \frac{1}{MN+1} \times \sum_{n=0}^{N-1}x(n)\left\{(1+2\sum_{j=1}^{N/2}\cos\frac{2\pi}{N}j\left(\frac{s}{M}-n\right)\right\}. \tag{11}$$

Equation (11) shows that in the time-domain interpolation, the interpolation is fulfilled by convoluting the original sequence with a coefficient. The coefficient only depends on M and s, where s ranges from 0 to $M \times N - 1$. Therefore, the parameter s/M can be any decimal fraction and it ranges from 0 to $N-1$ by changing M. The position s can be normalized to $s' = s/M$ by setting $M = 1$ in Eq. (11). As the discussion above, s' range from 0 to $N-1$. Finally, the time-domain interpolation can be obtained:

$$x_2(s') = \frac{1}{N+1} \times \sum_{n=0}^{N-1}x(n)\left\{1+2\sum_{j=1}^{N/2}\cos\frac{2\pi}{N}j(s'-n)\right\}. \tag{12}$$

Equation (12) shows that the resampled data can be obtained by a convolution in time-domain interpolation. This method needs $N \times N$ times' real-valued multiplication and the complex-value's multiplication in the zero-padding interpolation can be obtained by Eq. (13). So, this method is slower than zero-padding method if N is large

$$O(M,N) = \left(\frac{N}{2}\log_2 N\right) + \frac{MN}{2}\log_2 MN. \tag{13}$$

To get a further result, a coefficient formula is defined as:

$$C(n,s') = \frac{1}{N+1}\left(1+2\sum_{j=1}^{N/2}\cos\frac{2\pi}{N}j(s'-n)\right). \tag{14}$$

So, Eq. (12) can be written as:

$$x_2(s') = \sum_{n=0}^{N-1}x_1(n)C(n,s'). \tag{15}$$

Let $\Delta = s' - n$, the coefficient definition can be deduced as:

$$C(\Delta) = \frac{1}{N+1}\left(1+2\sum_{j=1}^{\frac{N}{2}}\cos\left(\frac{2\pi}{N}j\Delta\right)\right). \tag{16}$$

If positions s' is an integer, $\Delta = s' - n$ is also an integer. In this case, Eq. (16) can be expressed as:

$$C(\Delta) = \frac{1}{N+1}\left(1+\frac{2\sin(\frac{\pi}{2}\Delta)\cos(\frac{\pi}{2}\Delta+\frac{\pi}{N}\Delta)}{\sin(\frac{\pi}{N}\Delta)}\right), \tag{17}$$

when $\Delta = 0$, $C(\Delta) = 1$. Otherwise, $|C(\Delta)| = 1/(N+1)$. It means that when s' are integers, they are the original points and the points' original data contribute mainly to interpolation, other points have little influence on the interpolation and the influence decreases as N increases. On the other hand, if position s' is decimal, $\Delta = s' - n$ is decimal too. Thus, Eq. (16) can be expressed as

$$C(\Delta) = \frac{1}{N+1}\left(1+\sin(\pi\Delta)\cot\left(\frac{\pi}{N}\Delta\right)-2\sin^2\left(\frac{\pi}{2}\Delta\right)\right), \tag{18}$$

and then:

$$C(\Delta) = \frac{1}{N+1} + \frac{\sin(\pi\Delta)\cot(\frac{\pi}{N}\Delta)}{N+1} - \frac{2\sin^2(\frac{\pi}{2}\Delta)}{N+1} \tag{19}$$

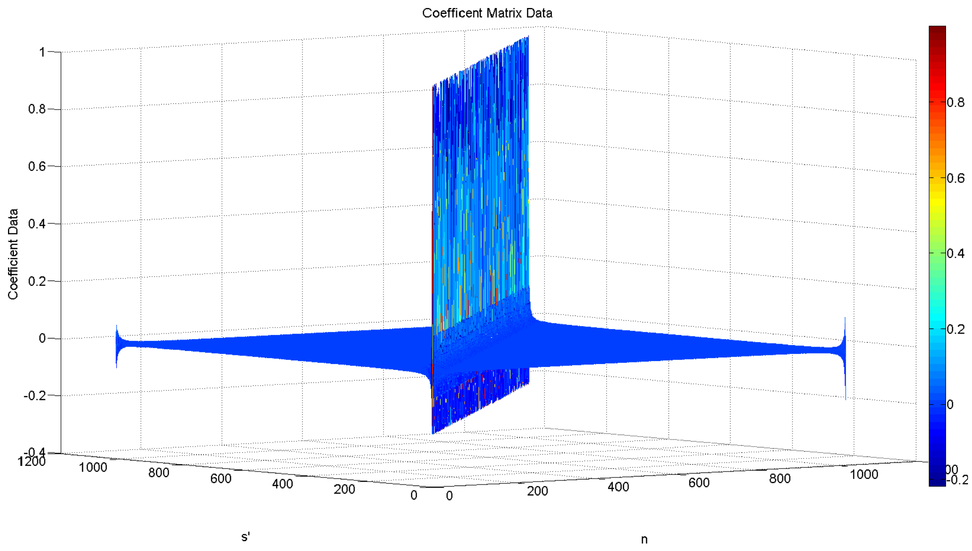

Fig. 1. Mesh of $C(\Delta)$ data with $N = 1024$.

The second term of Eq. (19) is a descending cotangent function modulated by a sine function. Its peak value is $N/(N+1)$ when Δ is any integer. Otherwise, the peak value is zero. Therefore, $C(\Delta)$ oscillate and decrease gradually as the absolute value of $\Delta(|\Delta|)$ increases.

The $C(\Delta)$ can be calculated by a random s' sequence. For example, Fig. 1 shows the $C(\Delta)$ with $N = 1024$.

Referring to Fig. 1 and Ref. 2, only a small number range coefficient $C(\Delta)$ mainly contribute to the interpolation. Therefore a narrow window can be used to symmetrically cut-off $C(\Delta)$ with an acceptable accuracy to reduce the computation time, whose middle point is located in the interpolation point. So the interpolation can be expressed as

$$x_2(s') = \sum_{n=\text{Begin}}^{\text{End}} x(n)C(n, s'), \tag{20}$$

where *Begin* and *End* represent the beginning and ending points of the cut-off window, respectively; $End{-}Begin = L$, with L representing the width of the cut-off window.

Quantitatively, the NMSE over the reconstruction window is defined as:

$$NMSE = \frac{\sum_{n=0}^{N-1} |x(n) - \hat{x}(n)|^2}{\sum_{n=0}^{N-1} |x(n)|^2}, \tag{21}$$

where $x(n)$ is the original sequence, $\hat{x}(n)$ is the sequence in the cut-off window. Assume there is a random sequence of s' and an $N \times N$ coefficient matrix can be obtained by Eq. (21). Table 1 presents the mean NMSE obtained with different N and L.

Table 1. The mean NMSE of the cut-off effect.

NMSE	$N = 1024$	$N = 2048$
$L = 11$	0.018561	0.0184183
$L = 21$	0.009689	0.0096148
$L = 31$	0.006545	0.0065043

Referring to Table 1 and Ref. 2, a few points occupy the most power of the coefficient. Therefore, a short-width window can be used to cut off the coefficient. By doing this, the accuracy is somewhat compromised. However, the processing time is significantly reduced. The cut-off width L is determined by a trade-off between the accuracy and the computation time. Referring to Eq. (13), the zero-padding interpolation needs 64,512 times complex multiplication (258,048 times real multiplication) if $N = 2048$ and $M = 4$. However, in the time-domain method only $N \times L = 22528$ times real times multiplication are needed if the cut-off width is $L = 11$. The computation time is reduced by more than 10 times. This would significantly speed up the system's processing speed and reduced the computational complexity.

3. Numeric Simulation

Several interpolation methods are compared by numerical simulation to validate the time-domain interpolation. Assume that there is an interference spectrum with a Gaussian shape, whose central wavelength is 850 nm and the spectral profile is

$$I(\lambda) = 100 \times \exp\left(-\left(\frac{\lambda - \lambda_0}{\sigma}\right)^2\right) \times \left(1 + \cos\left(\frac{2\pi}{\lambda} z\right)\right), \tag{22}$$

where $\lambda = 850$ nm, $\sigma = 25$ and z are the different distance mismatch. The spectrum's wavelengths evenly spread from 800 nm to 900 nm, but the corresponding wave numbers are not evenly spaced. Referring to the relationship between wavelength and wave number, the linearly wave number sequence can be obtained by the wavelength sequence. Thus, the interpolation can be applied by the wave number and wavelength sequence. Numerical simulations are performed with different z, N, M and L values.

The zero-padding method cannot be directly used to resample the data. So, a linear interpolation after zero-padding is needed. On the other hand, the time-domain interpolation can be performed directly.

The computing time is acquired to compare the interpolation speed. Since the interpolation time depends on the personal computer's capability, a computation time reduction factor is defined as $R = t_f/t_c - 1$ with t_f and t_c the computation time for the $M = 4$ interpolation and the time-domain interpolation, respectively.

Table 2 shows that the time-domain interpolation with all coefficient ($L = N$) is computational complexity, which consumes almost ten times than the zero-padding method. But the cut-off coefficient method can significantly reduce the processing time. The highest reduction factor is 6.70 when the cut-off width is 11 and $N = 1024$. Other factors decrease as the cut-off width increase.

The NMSE can be applied to evaluate the accuracy by supposing the original data and the interpolation data as $x(n)$ and $\hat{x}(n)$, respectively. Figure 2 shows the NMSE results. The time-domain interpolation with full coefficient ($L = N$) keeps the NMSE values stable with distance mismatch change, much higher than that of zero-padding method, but its computing time is larger too. The NMSE values of the time-domain interpolation with cut-off window oscillate when the distance mismatch change. The accuracy of the cut-off coefficient method ($L = 11$) is lower than that of zero-padding method ($M = 4$), but ($L = 21$) and ($L = 31$) can improve about 1.7 dB and 2.1 dB than that of zero-padding method ($M = 4$) at the distance mismatch $z = 2.4$ mm when $N = 2048$, respectively. Thus, the accuracy of time-domain interpolation increases as the cut-off width increasing. But the computing time of the cut-off coefficient increase as cut-off width increasing too. So, a trade-off between accuracy and computing speed should be taken.

4. System Experiment

The time-domain interpolation is applied to a SD-OCT system. The experimental setup is shown in Fig. 3. The light source is an SLD (Superlum, Russia, SLD 371-HP1) with a bandwidth of 45 nm FWHM at 840 nm. The spectrometer consists of a linescan camera (AVVIVA, SM2 CL 2014, 28 KHz at 2048 pixels), a transmission grating [Wasatch Photonics, 1200 (lines × pairs)/mm at 830 nm], and an achromatic lens ($f = 150$ mm). The galvo mirror is driven by the waveform generated by a function generation card (PCI 6122, National Instrument), the image acquisition car (IMAQ) (PCIe 1430,

Table 2. Computing time of different interpolation methods.[a]

		$N = 1024$		$N = 2048$	
		Time (ms)	R	Time (ms)	R
Zero-padding interpolation	$M = 4$	1.826	—	3.122	—
with linear interpolation	$M = 2$	1.007	—	1.942	—
	$L = N$	16.35	—	29.50	—
Time-domain interpolation	$L = 11$	0.237	6.70	0.414	6.54
with cut-off coefficient	$L = 21$	0.329	4.55	0.541	4.77
	$L = 31$	0.423	3.32	0.670	3.66

[a] *Note*: The personal computer platform: CPU: Intel Q9600 2.66 GHz; memory: 2G DDR2 800; operating system: Microsoft Windows 7; Developing platform: Microsoft Visual Studio 2005 SP1.

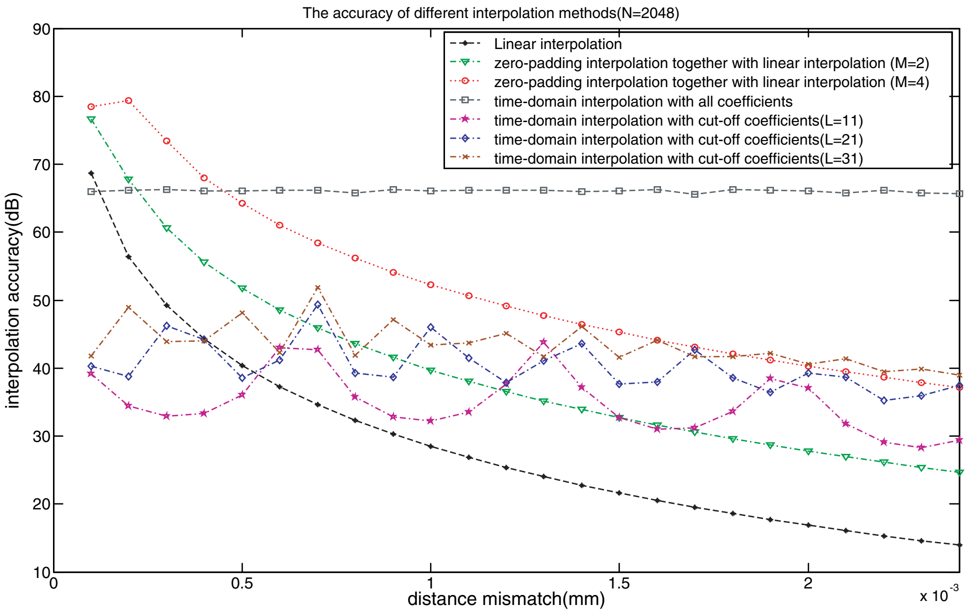

Fig. 2. The accuracy of different interpolation methods. The y-axis is the NMSE values by using the equation $-10 \times \log 10$ (NMSE).

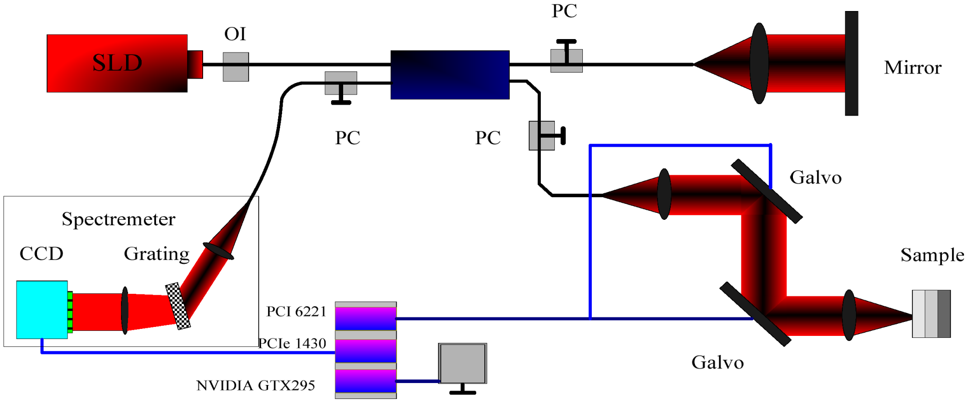

Fig. 3. SD-OCT setup: SLD, superluminescent diode; PC, polarization controller; OI, optical isolator.

National Instrument) acquire the interference data. The spectrometer must be calibrated before using the time-domain interpolation. The interpolation positions can be obtained by the calibration.[2,22,26,27] The interpolation accuracy can be evaluated by the fall-offs of the SD-OCT.[2] The fall-off of the SD-OCT is defined as:

$$20 \times \log 10[\text{abs}(\text{FFT}(\text{spectrum}))]. \qquad (23)$$

The fall-offs of the original data, the resampled data by zero-padding interpolation ($M = 2$ and $M = 4$) and the data by the proposed method ($L = 11$, $L = 21$ and $L = 31$) have been calculated in Ref. 2. A maximum fall-off improvement of ∼2 dB can be measured in the deep z positions between the proposed method ($L = 21$) and the zero-padding method ($M = 4$).[2] This is consistent with the numerical simulation. So, $L = 21$ is suitable for the time-domain interpolation in SD-OCT.

Moreover, Eq. (19) shows that time-domain interpolation only need a few raw data and the coefficient ranged in the cut-off window to obtained resampled data. A lot of points can be interpolated simultaneously. Therefore, a parallel algorithm can be applied to resample the data. This is suitable for the architecture of the GPU. A CUDA program is developed to accelerate the data processing of the SD-OCT. In our system, the program only uses a single core on a two cores GPU (NVIDIA, GeForce GTX 295).

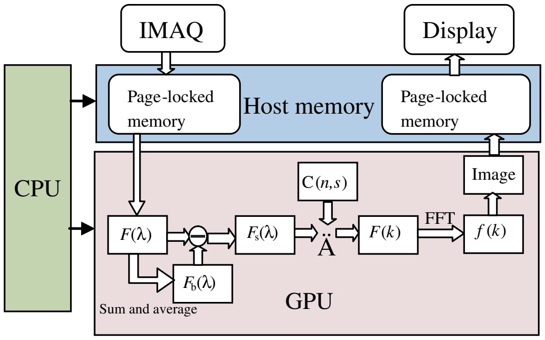

Fig. 4. Software architecture of the data processing for the SD-OCT system.

Figure 4 shows the software architecture of the data processing for the SD-OCT system. In order to fully utilize the capability of the GPU, the whole data processing including DC removal, spectrum resampling, inverse Fourier transform and image mapping, can be processed on GPU after transferring the needed data to GPU; $F_b(\lambda)$ is the DC component of the SD-OCT system, which can be obtained by averaging the spectral within an individual B scan.[28] Because coefficient $C(n, s)$ is independent of the acquired data, it can be computed and stored before system operating. Three steps are performed to obtain $\mathrm{C}(n, s)$.[2]

(1) The spectrometer must be calibrated by a standard calibration source before the system operating, obtaining a wavelength sequence corresponding to CCD pixels. This wavelength sequence is evenly spaced in λ space.

(2) A wave number sequence is obtained by the wavelength. This wave number sequence is linear spaced in k space.

(3) A virtual position is obtained by mapping the wave number sequence to the CCD pixels. And then the coefficient $C(n, s)$ is computed by Eq. (16).

The DC removed interference signal $F_s(\lambda)$ is obtained by subtracting $F_b(\lambda)$ from $F(\lambda)$. And then, the time domain interpolation method is applied to resample the signal by convoluting the interference data $F_s(\lambda)$ and coefficient $C(n, s)$. Hence, the linear wave number data sequence $F(k)$ is obtained. Finally, an image map processing is applied to get the B-scan image after the FFT operation.

An experiment is performed to test the processing capability of the GPU. The computing time includes the time of acquire data transfer from CPU to GPU, DC removal, spectrum resampling, inverse Fourier transform, image mapping and image data transfer from GPU to CPU. Figure 5 shows the results. It can be seen as a linear increase as the A-scan lines increase. Theoretically, the processing capability can be achieved 164,000 line/s for 1024 pixel OCT (1024-OCT) and 71,000 line/s for 2048 pixel OCT (2048-OCT) when the cut-off length is 21. A higher processing capability can be achieved 226,000 line/s for 1024-OCT and 104,000 line/s for 2048-OCT when the cut-off length is 11. But this speed is fast enough for the current linescan camera. It should be noted that the CPU and the GPU used in this system are not the professional devices. The

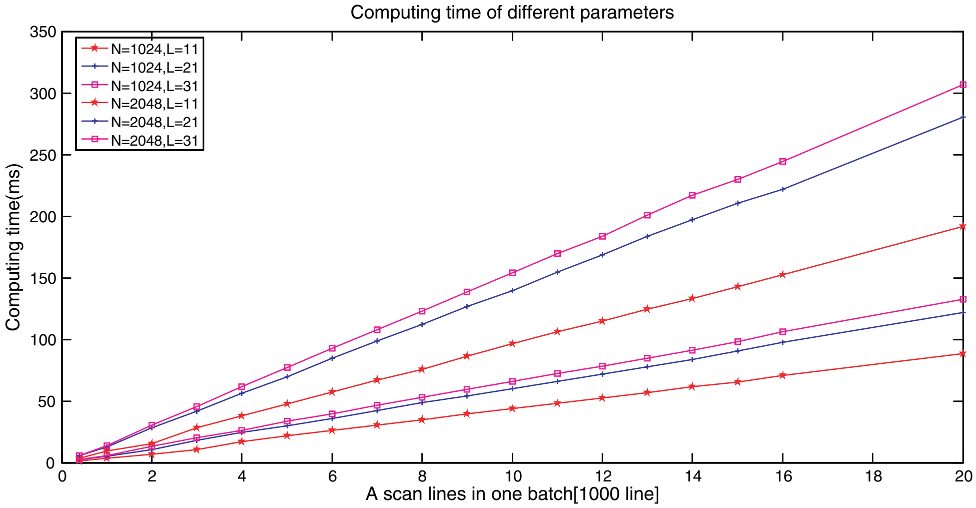

Fig. 5. GPU computing time of different parameters. The personal computer platform: CPU, Intel Q9600 2.66 GHz; memory 2G DDR2 800; GPU, NVIDIA GTX 295.

Table 3. Data processing time of different methods.

	GPU(ms)	CPU(ms)	R^{a}
Zero-Padding ($M = 4$)	15.01	326	20.72
Cut-off coefficient method ($L = 11$)	3.58	134	36.43
Cut-off coefficient method ($L = 21$)	5.46	150	26.47
Cut-off coefficient method ($L = 31$)	6.83	197	32.79

[a] *Note*: $R = t_f/t_c - 1$, with t_f and t_c the data processing time on CPU and the data processing time on GPU, respectively.

speed would be faster if the two cores are used or multiple GPUs are used.

A comparison of signal processing speed between the time-domain interpolation and the zero-padding is performed. A frame data (400 A-lines × 2048 pixels × 12 bits) is acquired and processed on GPU and CPU, respectively. Table 3 shows the results. The data processing time of the time-domain interpolation with cut-off coefficient method ($L = 21$) on GPU can be finished in 5.46 ms, much less than that on CPU. Moreover, the factor R of the time-domain methods is larger than that of the zero-padding method, which means that it is more suitable for parallel algorithm.

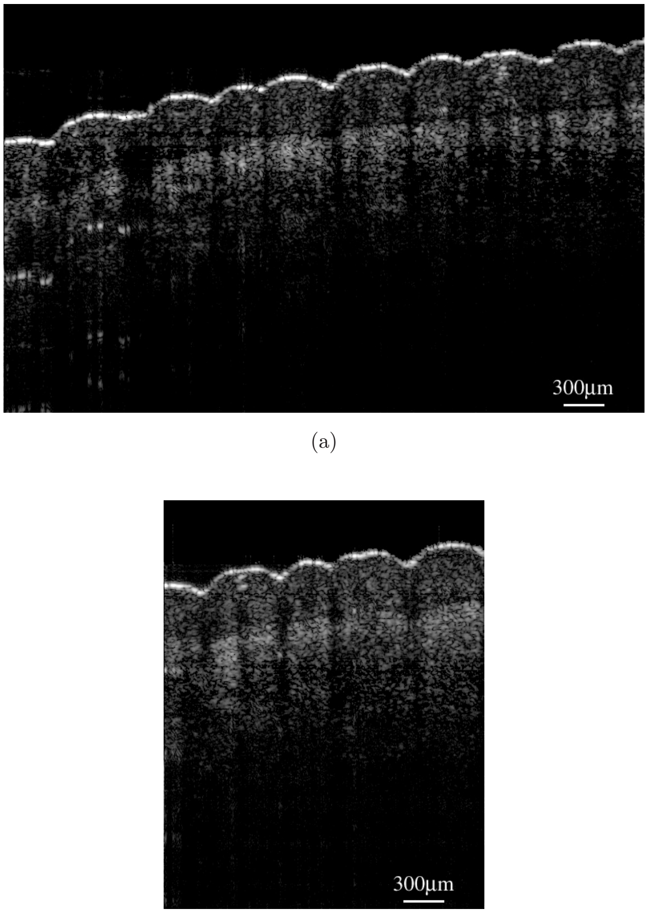

(a)

(b)

Fig. 6. Structure images of finger skin; (a) 800 A-lines × 2048 pixels × 12 bits; (b) 400 A-lines × 2048 pixels × 12 bits.

A finger has been scanned to validate the results. The scan frame of FD-OCT system is set to 800 A-lines × 2048 pixels × 12 bits and 400 A-lines × 2048 pixels × 12 bits, respectively. The cut-off width is set to 21. The corresponding frame rates are 20 frames per second and 40 frames per second, which is limited by the speed of the galvo mirror. Figure 6 shows the imaging results.

5. Conclusion

In this article, the essential steps of time-domain interpolation are discussed. A numerical simulation has been performed to compare the interpolation accuracy of the time-domain method and the zero-padding method. The time-domain interpolation reduced the interpolation position error by eliminating the linear interpolation, resulting in higher interpolation accuracy. The numerical simulation results shows that the cut-off coefficient method ($L = 21$) obtain about 1.7 dB accuracy improvement in the large distance mismatch than that of zero-padding interpolation method. This result matches the improvement reported in Ref. 2. Additionally, the time-domain method bypasses the huge FFT operations and interpolates data in time domain, obtaining higher interpolation speed than zero-padding interpolation method. The processing speed of the proposed method can accelerate more than three times than that of zero-padding interpolation method. Thus, it can realize a balance between the interpolation accuracy and the interpolation speed. Furthermore, the time-domain interpolation can be performed in parallel because the interpolation only relates to the coefficient and the data range in the cut off window. In order to make use of this advantage, a CUDA program is developed on GPU to accelerate the processing speed, reducing the data processing time greatly. The experiment result shows that the processing time can be reached more than 164,000 line/s for 1024-OCT and 71,000 line/s for 2048-OCT when the cut-off length is 21 and 226,000 line/s for 1024-OCT and 104,000 line/s for 2048-OCT when the cut-off length is 11. These speeds are much faster than the acquisition speed of the linescan camera.

An experiment is performed to acquire a frame data and process on GPU and CPU, respectively. The speed-up ratio shows that the time-domain interpolation is more suitable for parallel computing than the zero-padding interpolation method. In conclusion, the time-domain interpolation is a high-accuracy, high-processing speed and high-parallel computing ratio interpolation method. Hence, a high-sensitivity and high-speed data processing for nonlinear-K spectrometer SD-OCT can be realized by this time-domain interpolation.

Acknowledgments

We gratefully acknowledge the help of Prof. Wenhan Jiang and Prof. Bincheng Li from Institute of Optics and Electronics, Chinese Academy of Sciences. This work is supported by National High Technology R&D project of China (No. 2008AA02Z422) and The Instrument Developing Project of The Chinese Academy of Sciences, Institute of Optics and Electronic, Chinese Academy of Sciences.

References

1. D. Huang, E. A. Swanson, C. P. Lin, J. S. Schuman, W. G. Stinson, W. Chang, M. R. Hee, T. Flotte, K. Gregory, C. A. Pulifito, "Optical coherence tomography," *Science.* **254**, 1178–1181 (1991).
2. Y. Zhang, X. Li, L. Wei, K. Wang, Z. Ding, G. Shi, "Time-domain interpolation for Fourier-domain optical coherence tomography," *Opt. Lett.* **34**, 1849–1851 (2009).
3. J. G. Fujimoto, Chapter 1 in *Handbook of Optical Coherence Tomography*, B. E. Bouma, G. J. Tearney, eds., Marcel Dekker, Inc. (2002).
4. R. Leitgeb, C. Hitzenberger, A. Fercher, "Performance of fourier domain vs. time domain optical coherence tomography," *Opt. Exp.* **11**, 889–894 (2003).
5. M. Choma, M. Sarunic, C. Yang, J. Izatt, "Sensitivity advantage of swept source and Fourier domain optical coherence tomography," *Opt. Expres.* **11**, 2183–2189 (2003).
6. S. Makita, "High-speed spectral-domain optical coherence tomography and in vivo human eye imaging," University of Tsukuba. DA04252(2006).
7. U. Haberland, P. Jansen, V. Blazek, H. J. Schmitt, "Optical coherence tomography of scattering media using frequency-modulated continuous-wave techniques with tunale near-infrared laser," *in Coherence Domain Optical Methods in Biomdical Science and Clinical Applications, Proc. SPIE.* **2981**, 20–28 (1997).
8. S. R. Chinn, E. A. Swanson, J. G. Fujimoto, "Optical coherence tomography using a frequency-tunable optical source," *Opt. Lett.* **22**, 340–342 (1997).
9. A. F. Fercher, C. K. Hitzenberger, G. Kamp, S. Y. El-Zaiat, "Measurement of intraocular distances by backscattering spectral interferometry," *Opt. Commun.* **117**, 43–48 (1995).
10. B. Potsaid, I. Gorczynska, V. J. Srinivasan, Y. Chen, J. Jiang, A. Cable, J. G. Fujimoto, "Ultrahigh speed spectral/fourier domain OCT ophthalmic imaging at 70,000 to 312,500 axial scans per second," *Opt. Express.* **16**, 15149–15169 (2008).
11. M. Wojtkowski, "High-speed optical coherence tomography: Basics and applications," *Appl. Opt.* **39**, D30–D61 (2010).
12. R. Leitgeb, W. Drexler, A. Unterhuber, B. Hermann, T. Bajraszewski, T. Le, A. Stingl, A. Fercher, "Ultrahigh resolution Fourier domain optical coherence tomography," *Opt. Express.* **12**, 2156–2165 (2004).
13. S. Yan, D. Piao, Y. Chen, Q. Zhu, "Digital signal processor-based real-time optical Doppler tomography system," *J. Biomed. Opt.* **9**, 454–463 (2004).
14. J. Su, J. Zhang, L. Yu, H. G. Colt, M. Brenner, Z. Chen, "Real-time swept source optical coherence tomography imaging of the human airway using a microelectromechanical system endoscope and digital signal processor," *J. Biomed Opt.* **13**, 030506 (2008).
15. T. E. Ustun, N. V. Iftimia, R. D. Ferguson, D. X. Hammer, "Real-time processing for Fourier domain optical coherence tomography using a field programmable gate array," *Rev. Sci. Instrum.* **79**, 114301 (2008).
16. G. Liu, J. Zhang, L. Yu, T. Xie, Z. Chen, "Real-time polarization-sensitive optical coherence tomography data processing with parallel computing," *Appl. Opt.* **48**, 6365–6370 (2009).
17. NVIDIA CUDA. http://developer.nvidia.com/object/cuda.html
18. NVIDIA CUDA Computer Unified Device Architecture: Programming Guide, Version 2.0beta2, June 2008.
19. Y. Watanabe, T. Itagaki, "Real-time display on Fourier domain optical coherence tomography system using a graphics processing unit," *J. Biomed. Opt.* **14**, 060506 (2009).
20. K. Zhang, J. U. Kang, "Real-time 4D signal processing and visualization using graphics processing unit on a regular nonlinear-k Fourier-domain OCT system," *Opt. Express*, **18**, 11772–11784 (2010).
21. Y. Watanabe, S. Maeno, K. Aoshima, H. Hasegawa, H. Koseki, "Real-time processing for full-range

Fourier-domain optical-coherence tomography with zero-filling interpolation using multiple graphic processing units," *Appl. Opt*, **49**, 4756–4762 (2010).

22. M. Wojtkowskj, R. Leitgeb, A. K. Y. Bajraszewski, A. F. Fercher, "In vivo human retinal imaging by Fourier domain optical coherence tomography," *J. Biomed. Opt.* **7**, 457–463 (2002).
23. Z. Hu, Y. Pan, A. M. Rollins, "Analytical model of spectrometer-based two-beam spectral interferometry," *Appl. Opt.* **46**, 8499–8505 (2007)
24. M. Wojtkowskj, R. Leitgeb, A. K. Y. Bajraszewski, A. F. Fercher, "In vivo human retinal imaging by Fourier domain optical coherence tomography," *J. Biomed. Opt.* **7**, 457–463 (2002).
25. C. Dorrer, N. Belabas, J.-P. Likforman, M. Joffre, "Spectral resolution and sampling issues in Fourier-transform spectral interferometry," *J. Opt. Soc. Am. B.* **17**, 1795–1802 (2000).
26. K. Wang, Z. Ding, "Spectral calibration in spectral domain optical coherence tomography," *Chin. Opt. Lett.* **6**, 902–904 (2008).
27. C. J. Sansonetti, M. L. Salit, J. Reader, "Wavelengths of spectral lines in mercury pencil lamps," *Appl. Opt.* **35**, 74–77 (1996).
28. R. K. Wang, Z. H. Ma, "A practical approach to eliminate autocorrelation artifacts for volume-rate spectral domain optical coherence tomography," *Phys. Med. Biol.* **51**, 3231–3239 (2006).